Component-Based Model for Single-Plate Shear Connections with Pretension and Pinched Hysteresis

Jonathan M. Weigand [1]

ABSTRACT

Component-based connection models provide a natural framework for modeling the complex behaviors of connections under extreme loads by capturing both the individual behaviors of the connection components, such as the bolt, shear plate, and beam web, and the complex interactions between those components. Component-based models also provide automatic coupling between the in-plane flexural and axial connection behaviors, a feature that is essential for modeling the behavior of connections under column removal. This paper presents a new component-based model for single-plate shear connections that includes the effects of pre-tension in the bolts and provides the capability to model standard and slotted holes. The component-based models are exercised under component-level deformations calculated from the connection demands via a practical rigid-body displacement model, so that the results of the presented modeling approach remains hand-calculable. Validation cases are presented for connections subjected to both seismic and column removal loading. These validation cases show that the component-based model is capable of predicting the response of single-plate shear connections for both seismic and column removal loads.

Keywords: Steel; Shear Tab; Connections; Robustness; Structural Integrity; Disproportionate Collapse; Seismic Loading; Gravity Framing; Force-Displacement; Moment-Rotation

INTRODUCTION

Large-scale tests of steel gravity framing systems have repeatedly demonstrated that steel gravity connections provide a critical contribution to the robustness of systems subjected to

[1]Ph.D., Research Structural Engineer, Engineering Laboratory, National Institute of Standards and Technology, Gaithersburg, MD, USA, Email: jonathan.weigand@nist.gov

extreme loads such as earthquakes, fire, and column removal. Large-scale tests of steel gravity framing systems under earthquake loads (Liu and Astaneh-Asl 1999) and column removal (Johnson et al. 2014; Johnson and Meissner 2015) have shown that the system robustness (i.e., the continued ability of the system to redistribute loads) is largely dependent on the capacity of the connections to remain intact after undergoing potentially large and highly-localized rotation and axial displacement demands which were not anticipated in their designs. However, accurately determining the behavior and capacity of the gravity connections under the demands resulting from extreme loads, particularly in the context of restraint supplied by interaction with the concrete slab and the surrounding structure, is not trivial. Because full-scale tests of gravity connections under earthquake and column removal demands remain limited to just a handful of connection configurations and load histories, to evaluate general structural robustness under extreme loads, researchers and engineers need accurate and validated analysis tools to simulate the connection behavior over a wide range of connections.

Including contributions from the steel gravity frames could be advantageous in the design and analysis of new structures. In the design of structures for seismic and/or wind loads, most steel buildings constructed in the United States are designed with distinct systems for resisting lateral loads and gravity loads. Even though the gravity load resisting system typically comprises the majority of the steel framing, for simplicity it is often ignored in the lateral design (with the gravity connections idealized as perfectly pinned). However, full-scale tests of bare-steel single-plate shear connections under earthquake loads have shown that the connections provide moment capacities on the order of 15 % to 20 % of their beam plastic moment capacities, and when composite with a concrete slab on steel deck provide capacities on the order of 30 % to 60 % of their beam plastic moment capacities (Liu and Astaneh-Asl 1999). Including contributions from the steel gravity frames when computing the capacity the lateral load resisting system during the design stage could reduce the cost of the overall structural system, making steel moment frame or braced frame buildings more

competitive with concrete buildings. On the other hand, even if the gravity connections are not included in the design of the lateral load resisting system, including their contributions in subsequent building analyses under amplified design loads (i.e., the Federal Emergency Management Agency (FEMA) P-695 methodology) could provide a quantifiable measure of the inherent robustness (or reserve capacity) in the structural system, a topic of widespread current interest in the structural engineering community. In fact, a recent study on 1-, 2-, 4-, and 8-story non-ductile steel moment framed buildings subjected to the FEMA P-695 "Far-Field" ground motion set showed that including the gravity frames in the building analysis reduced the probability of collapse by 45 % (on average), when compared with analyses of the moment frames only (Judd and Charney 2014).

Several researchers (e.g., Sadek et al. (2008), Wen et al. (2013b), Main and Sadek (2014), Weigand (2014)) have shown that detailed finite element models can accurately simulate the behavior of single-plate shear connections under earthquake loads and column removal scenarios, which are used to evaluate the potential for disproportionate collapse. However, such models may be mesh-dependent, prone to convergence failure (when solved implicitly), and may require detailed calibration of the material-level fracture behavior to adequately capture connection failure. Moreover, while such a detailed resolution may be attainable at the component or sub-system level, the need to model large structural systems makes detailed modeling of complete structural systems infeasible. Main and Sadek (2014) recognized these limitations, and used their detailed finite element models to develop a reduced-order modeling approach for single-plate shear connections. The reduced-order approach used a biaxial spring to represent each bolt row in the connection with the spring initial stiffness estimated based on linear regression of rotational stiffness data from seismic testing, and quadratic hysteresis with zero permanent deformation at zero load. Main and Sadek (2014) showed that a reduced-order modeling approach provided good agreement with push-down tests of two-span beam assemblies by Thompson (2009).

Other researchers (e.g., Liu and Astaneh-Asl (2004), Foley et al. (2006), Wen et al.

(2013a)) have formulated lumped plasticity models for the connection moment-rotation and axial behaviors as a simplified means to capture the connection response. Such models may provide a fairly complete description of the connection backbone response (and hysteretic behavior, depending on the model) under pure rotation, but they do not account for the interactions between the connection flexural and axial behaviors. Thus, they may not be appropriate for many realistic seismic analyses, as during an earthquake the gravity connections can be subjected to significant axial loads in addition to rotations (Astaneh-Asl 2005), and they are not appropriate for many column removal scenarios in which the development of catenary action requires the connections to accommodate large axial deformations in combination with large rotations (Sadek et al. (2008), Oosterhof and Driver (2012), Main and Sadek (2014), Weigand (2014)).

Component-based models, described in more detail in Section 3, provide a natural framework for capturing the complex behaviors of steel gravity connections, including both fastener and connected element deformations. They provide automatic coupling of the in-plane flexural and axial behaviors, and Elsati and Richard (1996) showed that component-based models could be used to generate pushover moment-rotation responses for a variety of connections, when strength parameters were derived from the appropriate characteristic-width connection segments. Among others, Shen and Astaneh-Asl (2000) and Rassati et al. (2004) have successfully used component-based connection models in steel framing analyses.

A number of component-based models are already available in the literature for certain types of steel gravity connections (e.g., bolted end-plate and bolted angle connections), but models for single-plate shear connections are more limited. In addition to Main and Sadek (2014), described above, Elsati and Richard (1996) provided backbone response parameters for 76 mm (3.0 in) segments of single-plate shear connections and showed that component-based models could be used to simulate the connection pushover moment-rotation response. Weigand and Berman (2008) used component-based models to determine the moment-rotation response of single-plate shear connections, but with the backbone response

parameters taken from a bolt-bearing response curve developed by Rex and Easterling (1996), and incorporating multilinear hysteretic rules for the component unload/reload behaviors. Yu et al. (2009) also used the bolt-bearing curve developed by Rex and Easterling (1996) to model the backbone response of the connection segments to simulate the connection response under elevated temperatures, but with empirically modified stiffness values derived from finite element analysis results to model the temperature dependence. Most recently, Koduru and Driver (2014) modified the model from Yu et al. (2009) with different empirical calibration factors, and also included shear yielding and shear fracture, to simulate the response of single-plate shear connections under column removal.

This paper presents a new hysteretic component-based model for single-plate shear connections that can simulate the connection behavior under arbitrary in-plane load histories, thus providing a unified treatment of these connections for seismic loads and column removal scenarios. The component-based model also includes the effects of friction (due to bolt pretension) and slip to provide the capability to model connections with both standard and slotted holes. Multiple validation cases are presented, and the model is shown to provide close agreement with experimental results for single-plate shear connections under both seismic loads and column removal scenarios. The parameters of the model can be determined directly from the geometry and materials used in the connection design.

AVAILABLE UNIAXIAL MATERIAL MODELS

A number of uniaxial material models are available in the literature to simulate the material-level hysteretic behaviors of steel coupons and reinforcing bars. The three most commonly used models are the Ramberg-Osgood (Ramberg and Osgood 1943), Giuffré-Menegotto-Pinto (Giuffré and Pinto (1970), Menegotto and Pinto (1973)), and Richard-Abbott (Richard and Abbott 1975) models. The component-based connection model presented here makes use of the equation in Richard and Abbott (1975), commonly referred to as the "Richard Equation." Although the Richard Equation was originally formulated in terms of stress, strain, and elastic and plastic moduli, it can equivalently be used to express

the load R in terms of deformation Δ and elastic and plastic stiffnesses as:

$$R = \frac{(k_\mathrm{i} - k_\mathrm{p})\,\Delta}{\left(1 + \left|\frac{(k_\mathrm{i}-k_\mathrm{p})\Delta}{R_\mathrm{n}}\right|^n\right)^{(1/n)}} + k_\mathrm{p}\Delta \quad , \tag{1}$$

where k_i and k_p are elastic and plastic stiffnesses, respectively, n is a shape parameter that controls the sharpness of the transition from the elastic stiffness to the plastic stiffness, and R_n is a reference load, located at the projection of the plastic stiffness at a deformation of zero (Fig. 1(a)).

Eq. (1) was extended by Hsieh and Deierlein (1990) to allow for more general unload/reload behaviors via application of Masing's hypothesis. Masing's hypothesis states that, if the force-displacement response of a cyclically stabilized system at initial loading is described by the function

$$f\,(R, \Delta) = 0 \quad , \tag{2}$$

where R is the restoring force at displacement Δ, then the unload/reload branches of the steady-state hysteretic response are geometrically similar to the initial load curve, but magnified by a factor of 2. This statement is described by the equation

$$f\left(\frac{R - R_\mathrm{unl}}{2}, \frac{\Delta - \Delta_\mathrm{unl}}{2}\right) = 0 \tag{3}$$

where $(\Delta_\mathrm{unl}, R_\mathrm{unl})$ is the load reversal point for a particular loading branch. Applying Eq. (3) to Eq. (1) results in:

$$R\,(\Delta) = R_\mathrm{unl} + \frac{(k_\mathrm{i} - k_\mathrm{p})\,(\Delta - \Delta_\mathrm{unl})}{\left(1 + \left|\frac{(k_\mathrm{i}-k_\mathrm{p})(\Delta-\Delta_\mathrm{unl})}{2R_\mathrm{n}}\right|^n\right)^{(1/n)}} + k_\mathrm{p}\,(\Delta - \Delta_\mathrm{unl}) \quad . \tag{4}$$

which describes full hysteretic loops with no pinching and 'kinematic hardening' (i.e., translation of loops with increasing center displacements along the line defined by the plastic stiffness) (Fig. 1(b)).

Eq. (4) was further extended by Simões et al. (2001) to allow for an asymmetric hysteretic response by replacing the reference load of $2R_{\mathrm{n}}$ (in Eq. (4)) with a more general reference load, R_{cyc}, that updates upon each load reversal. For the most general behavior, the elastic and plastic stiffnesses, k_{i} and k_{p}, can also be updated at load reversal. The curve for a general load/unload branch thus becomes:

$$R\left(\Delta\right) = R_{\mathrm{unl}} + \frac{\left(k_{\mathrm{i}} - k_{\mathrm{p}}\right)\left(\Delta - \Delta_{\mathrm{unl}}\right)}{\left(1 + \left|\frac{\left(k_{\mathrm{i}} - k_{\mathrm{p}}\right)\left(\Delta - \Delta_{\mathrm{unl}}\right)}{R_{\mathrm{cyc}}}\right|^{n}\right)^{\left(1/n\right)}} + k_{\mathrm{p}}\left(\Delta - \Delta_{\mathrm{unl}}\right) \quad , \tag{5}$$

where $R_{\mathrm{cyc}} = R_{0A} + R_{0B}$, $k_{\mathrm{i}} = k_{\mathrm{i}}^{\mathrm{AB}}$, and $k_{\mathrm{p}} = k_{\mathrm{p}}^{\mathrm{AB}}$ for cycle A→B and $R_{0c} = R_{0B} + R_{cyc}$, $k_{\mathrm{i}} = k_{\mathrm{i}}^{\mathrm{BC}}$, and $k_{\mathrm{p}} = k_{\mathrm{p}}^{\mathrm{BC}}$ for cycle B→C, etc. (Fig. 1(c)).

COMPONENT-BASED CONNECTION MODEL

Component-based connection models provide a versatile analytical framework that can be used to model the responses of connections under extreme loads. In component-based connection models, the connection is discretized into multiple linear, multilinear, or nonlinear component springs assembled into a configuration that represents the geometry of the connection (Fig. 2), where each component spring embodies an isolated characteristic-width segment of a component of the connection (e.g., bolt, plate, angles, or beam web). To simulate the connection response, the component springs are attached to rigid links (representative of the framing members), which are permitted to displace and rotate relative to one another. Interactions between the component behaviors are simulated by analytically placing component springs in parallel or in series as appropriate, and the behavior of the connection is aggregated from the behaviors of the individual components from which it is comprised.

For the single-plate shear component-based model presented in this paper, the connection is notionally discretized into characteristic-width segments with aggregate force-displacement behaviors represented by discrete connection springs. Each characteristic-width segment contains contributions from a shear-plate segment, bolt shaft, and beam-web segment (Fig. 3(a)),

which are modeled as individual component springs in series as shown in Figs. 3(b) and 3(c). For simplicity, the plate spring in Fig. 3(b) is labeled as K^{+}_{plt}, representing the current stiffness of the shear plate in tension, and the plate spring in Fig. 3(c) is labeled as K^{-}_{plt}, representing the current stiffness of the shear plate in compression. Similar notation is used for the bolt and beam web springs.

Each component spring makes use of the most general form of the Richard Equation shown in Eq. (5) (i.e., the Richard Equation parameters are updated at each load reversal); however, the shear-plate and beam-web component spring behaviors each include an additional degree of generality, by letting the Richard Equation parameters be updated at the initiation of bearing deformations. The behavior of each component spring, including calculation of the parameters in the Richard Equation, is described in detail in the following sections.

Backbone Behavior of Shear Plate and Beam Web

The shear-plate and beam-web component springs (i.e., plate springs) are modeled using the same formulation, with responses that differ only as a result of differences in their input material properties and geometry. Their backbone curves are defined using a piecewise version of Eq. (5) as:

$$R\left(\Delta\right) = \begin{cases} \dfrac{\left(K^{-}_{\text{b}} - K^{-}_{\text{p}}\right)\left(\Delta - \Delta^{-}_{\text{br}}\right)}{\left(1 + \left|\dfrac{\left(K^{-}_{\text{b}} - K^{-}_{\text{p}}\right)\left(\Delta - \Delta^{-}_{\text{br}}\right)}{R^{-}_{\text{b}}}\right|^{n^{-}_{\text{b}}}\right)^{\left(1/n^{-}_{\text{b}}\right)}} + K^{-}_{\text{p}}\left(\Delta - \Delta^{-}_{\text{br}}\right) \ , & \Delta < \Delta_{\text{slipctr}} - \frac{1}{2}\Delta_{\text{slip}} \\ \dfrac{\left(K_{\text{i}} - K_{\text{y}}\right)\Delta}{\left(1 + \left|\dfrac{\left(K_{\text{i}} - K_{\text{y}}\right)\Delta}{R_{\text{y}}}\right|^{n}\right)^{\left(1/n\right)}} + K_{\text{y}}\Delta \ , & \Delta_{\text{slipctr}} - \frac{1}{2}\Delta_{\text{slip}} \leq \Delta \leq \Delta_{\text{slipctr}} + \frac{1}{2}\Delta_{\text{slip}} \\ \dfrac{\left(K^{+}_{\text{b}} - K^{+}_{\text{p}}\right)\left(\Delta - \Delta^{+}_{\text{br}}\right)}{\left(1 + \left|\dfrac{\left(K^{+}_{\text{b}} - K^{+}_{\text{p}}\right)\left(\Delta - \Delta^{+}_{\text{br}}\right)}{R^{+}_{\text{b}}}\right|^{n^{+}_{\text{b}}}\right)^{\left(1/n^{+}_{\text{b}}\right)}} + K^{+}_{\text{p}}\left(\Delta - \Delta^{+}_{\text{br}}\right) \ , & \Delta > \Delta_{\text{slipctr}} + \frac{1}{2}\Delta_{\text{slip}} \end{cases} \tag{6}$$

where the superscripts, $(\cdot)^{+}$ and $(\cdot)^{-}$, denote tensile and compressive deformations of the component spring, respectively. Fig. 4 shows a schematic of the backbone force-displacement behavior described by Eq. (6). Descriptions of the behaviors that make up the component

spring backbone curve are described in more detail below.

Friction-Slip Behavior

Prior to bearing, the single-plate shear connection resists load via friction due to the clamping force provided by the bolt pre-tension and the surface-to-surface contact between the bolt head and shear plate, bolt nut and beam web, and shear plate and beam web. For slip-critical connections, the plates behave elastically prior to slip, with initial stiffnesses determined from the gross areas of the plate characteristic-width segments as:

$$K_{\mathrm{i}} = \frac{w t_{\mathrm{p}} E}{a} \tag{7}$$

where w is the width of the shear plate, t_{p} is the plate thicknesses, E is the modulus of elasticity of steel, and a is the distance from the column face to the bolt line. Connections that do not use pre-tensioned bolts may not be able to develop the elastic plate stiffnesses, and thus may have significantly smaller initial stiffnesses. For connections without pre-tensioned bolts, the initial stiffness of the friction-slip behavior can be assumed as equal to the initial plate bearing stiffness for the relevant loading direction, K_{b}^{+} or K_{b}^{-}, defined below.

Slip occurs as the loading overcomes the frictional resistance supplied by the bolt pre-tension. After slip is initiated, the bolt continues to slip until the initiation of bearing contact between the bolt shaft and the faces of the bolt holes (i.e., at deformations of $\Delta_{\mathrm{slipctr}} - \frac{1}{2}\Delta_{\mathrm{slip}}$ in compression or $\Delta_{\mathrm{slipctr}} + \frac{1}{2}\Delta_{\mathrm{slip}}$ in tension, where Δ_{slip} is the difference between the plate hole diameter (or slot width, when applicable) and the bolt diameter). The deformation parameter, $\Delta_{\mathrm{slipctr}} \in \left[\Delta_{\mathrm{slipctr}} - \frac{1}{2}\Delta_{\mathrm{slip}}, \Delta_{\mathrm{slipctr}} + \frac{1}{2}\Delta_{\mathrm{slip}}\right]$, allows the slip deformations to be biased toward the tension or compression bearing portions of Eq. (6), which is, in effect, equivalent to biasing the center of the bolt shaft toward the tension or compression edges of the bolt holes.

The load at slip depends on the amount of pre-tension in the bolts and the coefficient of

friction between steel surfaces, and can be calculated as:

$$R_{\text{slip}} = n_{\text{f}} \mu \alpha A_{\text{b}} F_{\text{u,bolt}} \quad , \tag{8}$$

where μ is the coefficient of friction between the steel surfaces in contact, n_{f} is the number of faying surfaces (or slip planes), A_{b} is the bolt cross-sectional area, and α is the ratio of the bolt pre-tension load to the bolt tensile strength $F_{\text{u,bolt}}$. For the modeling presented in this paper, $\alpha = 0.75$ was used and μ was taken as 0.338, corresponding to an average value calculated from the data compiled by Grondin et al. (2007).

It should be noted that if the connections are loaded dynamically, the load in the connection spring may decrease as the coefficient of friction decreases from the static to the kinetic coefficient of friction. However, most tests of single-plate shear connections, including those used for validation of the proposed model, were conducted at sufficiently small loading rates that their behavior remained pseudo-static. For pre-tensioned bolts in pseudo-static tests, the resistance of the connection tends to remain relatively constant or even increase slightly as the bolts slip (e.g., Liu and Astaneh-Asl (2004), Weigand (2014)). While Eq. (6) actually allows for either positive or negative slip stiffnesses (designated as K_{y}), the validation studies presented here found that a small positive value of 0.01 % of the initial stiffness was appropriate in all of the considered cases.

Bearing Behavior

The bearing behavior of the bolt on the plate and beam web edge distances (i.e., the plate component spring bearing response in tension) was adapted from the work of Rex and Easterling (1996), who performed 46 tests of a single bolt bearing against a single-plate with varied edge distances, plate thicknesses, bolt diameters, plate widths, and edge conditions (sheared or sawed). Using normalized bearing force-deformation results from ten tests, Rex and Easterling (1996) fit the parameters of Eq. (1) to their data, using nonlinear least-squares

regression techniques, to establish the following behavioral model for the bearing response:

$$\frac{R}{\bar{R}_{\mathrm{b}}} = \frac{\left(\alpha_{k_{\mathrm{b}}} - \alpha_{k_{\mathrm{p}}}\right)\bar{\Delta}}{\left(1 + \left|\frac{\left(\alpha_{k_{\mathrm{b}}} - \alpha_{k_{\mathrm{p}}}\right)\bar{\Delta}}{\alpha_{r_{\mathrm{b}}}}\right|^{n}\right)^{(1/n)}} + \alpha_{k_{\mathrm{p}}}\bar{\Delta} = \frac{1.74\bar{\Delta}}{\left(1 + \bar{\Delta}^{(1/2)}\right)^{2}} - 0.009\bar{\Delta} \quad , \tag{9}$$

where $\alpha_{k_{\mathrm{b}}} = 1.731$, $\alpha_{k_{\mathrm{p}}} = -0.009$, $\alpha_{r_{\mathrm{b}}} = 1.740$, and $n = 1/2$ are fitted Richard Equation parameters to the normalized data and $R/\bar{R}_{\mathrm{b}}$ is the normalized bearing load. The parameter $\bar{R}_{\mathrm{b}} = L_{\mathrm{ehp}} t_{\mathrm{p}} F_{\mathrm{u}} \leq 2.4 d_{\mathrm{b}} t_{\mathrm{p}} F_{\mathrm{u}}$ is the nominal strength of the plate edge distance in bearing/tearout, where L_{ehp} is the plate horizontal edge distance, F_{u} is the plate tensile strength, d_{b} is the bolt diameter, and the $(\bar{\cdot})$ notation distinguishes $\bar{\Delta}$ and $\bar{R}_{\mathrm{b}}$ as belonging to the *normalized* bearing response in Rex and Easterling (1996). The normalized bearing deformation, $\bar{\Delta}$, is defined as

$$\bar{\Delta} = \beta_{\mathrm{s}} \left(\bar{K}_{\mathrm{b}}/\bar{R}_{\mathrm{b}}\right) \Delta \quad , \tag{10}$$

where Δ is the actual bearing deformation, β_{s} is a steel correction factor ($\beta_{\mathrm{s}} = 1$ for structural steel), and $\bar{K}_{\mathrm{b}}$ is the elastic stiffness of the of the normalized bearing force-deformation response, defined as

$$\bar{K}_{\mathrm{b}} = \left(\frac{1}{\bar{K}_{\mathrm{b}}^{\mathrm{br}}} + \frac{1}{\bar{K}_{\mathrm{b}}^{\mathrm{b}}} + \frac{1}{\bar{K}_{\mathrm{b}}^{\mathrm{v}}}\right)^{-1} \quad . \tag{11}$$

The stiffness contributions to the elastic bearing stiffness resulting from direct bearing ($\bar{K}_{\mathrm{b}}^{\mathrm{br}} = 120 t_{\mathrm{p}} F_{\mathrm{y}} d_{\mathrm{b}}^{(4/5)}$), bending ($\bar{K}_{\mathrm{b}}^{\mathrm{b}} = 32 E t_{\mathrm{p}} \left(L_{\mathrm{ehp}} - d_{\mathrm{b}}/2\right)^{3}$), and shearing ($\bar{K}_{\mathrm{b}}^{\mathrm{v}} = (20/3)\, G t_{\mathrm{p}} \left(L_{\mathrm{ehp}} - d_{\mathrm{b}}/2\right)$) were determined by Rex and Easterling (1996), by assuming that the plate horizontal edge distance acts as a small fixed-fixed beam undergoing flexural and shear deformations under uniform load. $G = E/\left(2\left(1+\nu\right)\right)$ is the plate shear modulus, ν is Poisson's ratio, and F_{y} is the plate yield strength.

For adaptation of Eq. (9) to the component-based model for single-plate shear connections, it is more convenient to express the bearing curve in terms of non-normalized stiffnesses, bearing load, and bearing deformation. Substituting the fitted Richard Equation

parameters and the definition for normalized deformation (Eq. (10)) into Eq. (9) gives:

$$R = \left[\frac{\left(\alpha_{k_\mathrm{b}} - \alpha_{k_\mathrm{p}}\right)\left(\beta\left(\frac{\bar{K}_\mathrm{b}}{\bar{R}_\mathrm{b}}\right)\Delta\right)}{\left(1 + \left(\frac{\left(\alpha_{k_\mathrm{b}} - \alpha_{k_\mathrm{p}}\right)}{r_\mathrm{b}}\left(\beta\left(\frac{\bar{K}_\mathrm{b}}{\bar{R}_\mathrm{b}}\right)\Delta\right)\right)^n\right)^{(1/n)}} + \alpha_{k_\mathrm{p}}\left(\beta\left(\frac{\bar{K}_\mathrm{b}}{\bar{R}_\mathrm{b}}\right)\Delta\right) \right] \bar{R}_\mathrm{b} \quad , \tag{12}$$

which can be written as

$$R = \frac{\left(K_\mathrm{b}^+ - K_\mathrm{p}^+\right)\Delta}{\left(1 + \left|\frac{\left(K_\mathrm{b}^+ - K_\mathrm{p}^+\right)\Delta}{R_\mathrm{b}}\right|^n\right)^{(1/n)}} + K_\mathrm{p}^+\Delta \quad , \tag{13}$$

where $K_\mathrm{b}^+ = \beta_\mathrm{s}\bar{K}_\mathrm{b}\alpha_{k_\mathrm{b}}$ and $K_\mathrm{p}^+ = \beta_\mathrm{s}\bar{K}_\mathrm{b}\alpha_{k_\mathrm{p}}$ are the actual elastic and plastic bearing stiffnesses of the bearing force-deformation response, $R_\mathrm{b}^+ = \bar{R}_\mathrm{b}\alpha_{r_\mathrm{b}}$ is the nominal bearing reference load, and the superscript $(\cdot)^+$ denotes positive deformation at the connection (i.e., tension, see Fig. 4 for more details). Eq. (13) is exactly equivalent to Eq. (9), but is now expressed in terms of the actual, rather than normalized, bearing deformation.

The bearing response of the plates in compression is more constrained than the bearing response in tension, due to the fixity of the plate welds and to the additional plate material in front of the bearing contact. The additional constraint suppresses the bending and shearing deformation modes of the plates at the bolt holes, leading to a marginally stiffer force-deformation response in compression, relative to that in tension. This asymmetric effect has also been noted experimentally for single-plate shear connections under increasing magnitude reversed cyclic loading (Crocker and Chambers 2004). Thus, the component spring bearing force-deformation response in compression was modified to mirror the response in tension, but with initial elastic and plastic bearing stiffnesses based only on direct bearing stiffness such that $K_\mathrm{b}^- = \beta_\mathrm{s}\bar{K}_\mathrm{b}^\mathrm{br}\alpha_{k_\mathrm{b}}$ and $K_\mathrm{p}^- = \beta_\mathrm{s}\bar{K}_\mathrm{b}^\mathrm{br}\alpha_{k_\mathrm{p}}$, and with $\alpha_{k_\mathrm{p}} = 0.001$ taken as a small positive value to avoid the potential for negative tangent stiffnesses.

Load Reversal Behavior of Shear Plate and Beam Web

The behavior of single-plate shear connections upon load reversal is typically nonlinear and can be relatively complex; however, adequately capturing those complexities is critical to modeling the history-dependent resistance and energy dissipation capacity of the connections. Tests on single-plate shear connections under seismic loads include many load reversals, and results have shown that while the connection moment-rotation response has relatively little pinching at small rotations, the response becomes increasingly pinched and nonlinear at large rotations (e.g., Crocker and Chambers (2000), Liu and Astaneh-Asl (2004)). Also, although not as obvious, capturing the component-spring-level load reversal and accurate hysteresis behavior is important in modeling the behavior of connections under column removal (Main and Sadek 2014). Column removal tests on steel framed systems subject the connections to large rotation demands in combination with large axial deformation demands. Though these demands are often monotonically increasing until failure, axial connection spring displacements calculated in connection sub-assemblage experiments by Weigand and Berman (2014) have shown that connection characteristic-width segments that were initially bearing in compression will transition to tension as the connection transitions from flexure-dominated to tension-dominated (or catenary-type) behavior. Connection failure may also initiate load reversals. For example, after bolts shear, connection characteristic-width segments that were in tension prior to the failure may shift back to compression in order to accommodate the redistribution of flexural loads among the remaining intact bolt width segments. These considerations motivate the need for models that can adequately capture both load reversal and pinched hysteresis.

Load Reversal Prior to Bearing

The friction supplied by pre-tensioned bolts resists sliding in both directions equally. In the plate component springs, the cyclic friction slip behavior at load reversal is characterized

by

$$R(\Delta) = R_{\text{unl}} + \frac{(K_{\text{i}} - K_{\text{y}})(\Delta - \Delta_{\text{unl}})}{\left(1 + \left|\frac{(K_{\text{i}} - K_{\text{y}})(\Delta - \Delta_{\text{unl}})}{R_{\text{cyc}}}\right|^{n_{\text{y}}}\right)^{(1/n_{\text{y}})}} + K_{\text{y}}(\Delta - \Delta_{\text{unl}}) \quad , \tag{14}$$

where $(\Delta_{\text{unl}}, R_{\text{unl}})$ are the coordinates of the last unload point and $R_{\text{cyc}} = \text{sign}(\Delta - \Delta_{\text{unl}})R_{\text{y}} - R_{\text{unl}} + K_{\text{y}}\Delta_{\text{unl}}$ is the updated value of the cyclic reference load. Eq. (14) represents a full cyclic hysteresis symmetric about the origin. Fig. 5 shows an example of the connection spring response undergoing multiple cycles prior to bearing, with deformations contributed by both the shear plate and beam web component springs.

Load Reversal After Bearing

After bearing has been initiated, the plate component spring model tracks the coordinates of the last unload point, as well as the coordinates of the minimum and maximum unload points, $(\Delta_{\text{unl,min}}, R_{\text{unl,min}})$ and $(\Delta_{\text{unl,max}}, R_{\text{unl,max}})$, respectively. The load reversal behavior is then defined between the current values of the minimum and maximum unload points, permitting the model to capture the evolution of the connection response with increased hole elongations (i.e., as bearing deformations are accumulated). This aspect of the model is critical to modeling the seismic response of connections subjected to increasing magnitude rotation cycles.

Pinching begins in the connection at the initiation of bearing deformations. The increased pinching at large rotations occurs as a result of the loss of pre-tension in the bolts with increased bearing deformations. In the connection model, this phenomenon is captured within the shear-plate and beam-web component springs by allowing the pinching to vary as a function of accumulated bearing deformation. The formulation for the pinched hysteresis uses a combination of two curves to calculate the model response. Both curves originate at the previous load reversal point. The first curve is the general form of the Richard Equation, written in terms of the bearing curve parameters. For unload from a load reversal point in

tension, the Richard Equation is:

$$R\left(\Delta\right) = R_{\text{unl}} + \frac{\left(K_{\text{b}}^{+} - K_{\text{p}}^{+}\right)\left(\Delta - \Delta_{\text{unl}}\right)}{\left(1 + \left|\frac{\left(K_{\text{b}}^{+} - K_{\text{p}}^{+}\right)\left(\Delta - \Delta_{\text{unl}}\right)}{R_{\text{cyc}}}\right|^{n_{\text{b}}^{+}}\right)^{\left(1/n_{\text{b}}^{+}\right)}} + K_{\text{p}}^{+}\left(\Delta - \Delta_{\text{unl}}\right) \quad , \tag{15}$$

where $R_{\text{cyc}} = R_{\text{b}}^{+} + R_{\text{y}}$ for the initial unload cycle, and $R_{\text{cyc}} = R_{\text{unl,max}} - R_{\text{unl,min}}$ for all subsequent cycles. Eq. (15) represents a "full" hysteretic response (i.e., load reversal behavior with no pinching) as illustrated in Fig. 1(b).

The second curve defined between load reversal points is a polynomial known as the Bézier curve (e.g., Farin (1993), Prautizsch et al. (2002)). The Bézier curve was chosen because it provides an adaptable smoothly transitioning approximation to a piecewise-linear curve. The Bézier curve is defined such that it traverses a path through zero load at zero displacement and terminates at the previous minimum or maximum unload point, depending on loading direction. The Bézier curve is calculated as

$$\mathbf{B}(t) = \sum_{i=0}^{n} B_i^n(t)\mathbf{P}_{\text{i}} \quad , \tag{16}$$

where t is a parametric variable ranging from 0 to 1 (i.e., 0 at the current unload point and 1 at the current reload point),

$$B_i^n = \binom{n}{i}(1-t)^{n-i}t^i \qquad i = 0, 1, \ldots, n \tag{17}$$

are Bernstein polynomials, $\binom{n}{i} = \frac{n!}{i!(n-i)!}$ are the binomial coefficients, and $\mathbf{P}_{\text{i}}$ is the set of control points that define the curve trajectory (Fig. 6). The control points are defined along three segments. The first segment unloads from the current load reversal point at the initial bearing stiffness. The second segment initiates at the intersection of the first segment with a small residual stiffness segment that passes through zero and terminates at its

intersection with a reload segment. The reload segment has reload stiffness, K_{rel}, intersecting the backbone curve at the relevant maximum or minimum unload point. Detailed processing of the data in Liu and Astaneh-Asl (1999) showed that $K_{\text{rel}}^{-} = (1/2)\, K_{\text{b}}^{-}$ and $K_{\text{rel}}^{+} = (1/2)\, K_{\text{b}}^{+}$ provide reasonable initial values, and that the reload stiffness degraded at large rotations.

At a given value of t, the Bézier curve resulting from Eq. (16) has two components. The first component corresponds to the component spring axial deformation, $\mathbf{B}_1(t) = \Delta$, and the second component corresponds to the component spring load, $\mathbf{B}_2(t) = R_{\text{BZ}}$. The loads calculated from Eq. (16) represent load reversal behavior that is fully pinched.

The actual load reversal behavior is calculated as a weighted summation between the full hysteretic (i.e., Richard Equation) and fully pinched (i.e., Bézier curve) behaviors as:

$$R_{\text{p}} = \gamma R + (1 - \gamma)\, R_{\text{BZ}} \quad , \tag{18}$$

where the amount that each curve contributes to the response defines the pinching ratio γ, which can vary between 0 and 1. When $\gamma = 1$, the model is not pinched and $R_{\text{p}}(\Delta) = R(\Delta)$. When $\gamma = 0$, the model is fully pinched, and $R_{\text{p}}(\Delta) = R_{\text{BZ}}(\Delta)$. Similarly, a pinching ratio of 0.5 indicates that the model is pinched and will have a load equal to 50 % of the full hysteresis response at the crossover displacement (i.e., the value of zero displacement when crossing from positive to negative or negative to positive deformations). Fig. 7(a) shows a schematic of the pinching behavior for the initial unload cycle and Fig. 7(b) shows a schematic of the pinching behavior for the subsequent cycles.

Fig. 8 shows an unload/reload cycle of the actual connection spring response with pinching contributed by both the shear-plate and beam-web component springs when $\gamma = 0.5$ (representative of a cycle initiated after significant accumulated bearing deformation has already occurred). As Fig. 8 demonstrates, the formulation outlined in this section results in a pinched hysteresis with small residual stiffness at the crossover displacement, with a smooth transition between unload and reload points.

Calibration of Pinched Hysteresis

The evolution of the pinching was determined by assuming that the bolt behaves elastically, and calibrating the shear-plate and beam-web component-spring pinching behavior against data from Liu and Astaneh-Asl (2004), for a four-bolt single-plate shear connection subjected to increasing magnitude rotation cycles. For each half-cycle (i.e., peak to valley or valley to peak), the value of the pinching parameter γ was iterated until the load at the cross-over displacement in the model (i.e., the load at a displacement of zero) matched that of the test within a specified tolerance. The results of the pinching calibration are shown in Fig. 9, as a function of accumulated bearing deformation in the shear-plate component spring. A smooth lower-bound curve was fitted to the pinching data to generalize the pinching behavior for subsequent analyses. Fig. 10 shows a comparison of the model response using the calibrated pinching function to experimental data from Liu and Astaneh-Asl (2004). Fig. 10 demonstrates that use of the fitted lower-bound pinching curve qualitatively captures the increased pinching at large rotations, providing a reasonable approximation to the pinching behavior exhibited by the connection test.

Bolt Behavior

The transverse force-deformation behavior of the bolt, including shear and flexural effects, is modeled using Eq. (5) with the relevant bolt elastic and plastic shear stiffnesses, as:

$$R_{\text{bolt}}\left(\Delta\right) = R_{\text{unl}} + \frac{\left(K_{\text{i,bolt}} - K_{\text{p,bolt}}\right)\left(\Delta - \Delta_{\text{unl}}\right)}{\left(1 + \left|\frac{\left(K_{\text{i,bolt}} - K_{\text{p,bolt}}\right)\left(\Delta - \Delta_{\text{unl}}\right)}{2R_{\text{cyc,bolt}}}\right|^{n_{\text{bolt}}}\right)^{\left(1/n_{\text{bolt}}\right)}} + K_{\text{p,bolt}}\left(\Delta - \Delta_{\text{unl}}\right) \quad , \quad (19)$$

where $(\Delta_{\text{unl}}, R_{\text{unl}})$ are the coordinates of the last unload point, $n_{\text{bolt}} = 2$, $R_{\text{cyc,bolt}} = \text{sign}(\Delta - \Delta_{\text{unl}})R_{\text{v,bolt}} - R_{\text{unl}} + K_{\text{p,bolt}}\Delta_{\text{unl}}$, and $R_{\text{v,bolt}} = 0.62A_{\text{bolt}}F_{\text{u,bolt}}$ is the shear capacity of the bolt. Eq. (19) is applicable to both ASTM A325 (ASTM 2014b) and ASTM A490 (ASTM 2014a) structural bolts. Fig. 11(a) shows a comparison of the bolt component spring backbone force-displacement response to data from three bolt shear tests for 19.1 mm (¾ in) diameter

A325 bolts from Weigand and Berman (2014), and Fig. 11(b) shows the behavior of the bolt spring under increasing magnitude cyclic deformations.

The initial stiffness of the bolt force-deformation response is calculated using the assumption of springs in series as

$$K_{\mathrm{i,bolt}} = \frac{1}{\frac{1}{K_{\mathrm{br,bolt}}} + \frac{1}{K_{\mathrm{v,bolt}}}} \quad . \tag{20}$$

where $K_{\mathrm{br,bolt}}$ is the bolt bearing stiffness and $K_{\mathrm{v,bolt}}$ is the bolt shearing stiffness. The bearing stiffness is calculated as

$$K_{\mathrm{br,bolt}} = \frac{1}{1 + 3\beta_{\mathrm{b}}} \left(\frac{t_{\mathrm{p}} t_{\mathrm{w}} E_{\mathrm{bolt}}}{2 t_{\mathrm{p}} t_{\mathrm{w}}} \right) \quad , \tag{21}$$

based on the work by Nelson et al. (1983), where β_{b} is a correction factor that accounts for the concentration of bearing forces at the interface between plates for bolts in single shear. The value of β_{b} can range from 1 for a simple shear pin to relatively small values on the order of 0.15 for pre-tensioned bolts with large bolt heads, washers, and nuts. For the analyses presented below, a value of $\beta_{\mathrm{b}} = 0.7$ was found to provide the appropriate bolt bearing stiffness. The bolt shearing stiffness is determined by assuming that the bolt acts as a prismatic Timoshenko beam with circular cross-section and fixed ends, such that:

$$K_{\mathrm{v,bolt}} = \frac{12 E_{\mathrm{bolt}} I_{\mathrm{bolt}}}{L_{\mathrm{bolt}}^3 (1 + \Phi)} \quad , \tag{22}$$

where E_{bolt} is the bolt modulus of elasticity, $I_{\mathrm{bolt}} = {}^{\pi d_{\mathrm{b}}^4}/_{64}$ is the moment of inertia of the bolt shaft cross-section, $L_{\mathrm{bolt}} = t_{\mathrm{p}} + t_{\mathrm{w}}$ is the bolt length, and

$$\Phi = \frac{12 E_{\mathrm{bolt}} I_{\mathrm{bolt}}}{L_{\mathrm{bolt}}^2 \left(\frac{1}{\kappa G_{\mathrm{bolt}} A_{\mathrm{bolt}}} \right)} \tag{23}$$

is a term in Timoshenko beam theory that characterizes the relative importance of the shear deformations to the bending deformations (Thomas et al. 1973). In Eq. (23), $G_{\mathrm{bolt}} = {}^{E}/_{2\,(1+\nu)}$

is the bolt shear modulus, $A_{\text{bolt}} = (\pi/4)\, d_{\text{b}}^2$ is the bolt area, and κ is the shear coefficient for a circular cross-section, defined as:

$$\kappa = \frac{1}{\frac{7}{6} + \frac{1}{6}\left(\frac{\nu}{1+\nu}\right)^2} \quad . \tag{24}$$

The bolt plastic shear stiffness, $K_{\text{p,bolt}}$, was calculated as 2 % of the bolt initial shear stiffness, $K_{\text{i,bolt}}$, based on the measured values from the bolt shear data shown in Fig. 11(a).

Selection of Material Properties

The selection of proper material properties for the model depends on the intended application. If the intended usage is as a behavioral model (i.e., to predict the expected behavior or performance of the connection), then material properties determined from ASTM International material testing of the actual shear plate, beam web, and bolts used in the connection are appropriate. If material tests are not available, then the material properties listed on the mill certifications for the actual batches of steels used in the connection provide a reasonable alternative. In lieu of material tests or mill certifications, the expected material strengths for structural steels listed in ANSI/AISC 341-10 - Seismic Provisions for Structural Steel Buildings (AISC 2005) do result in a reasonable connection response, but may overestimate the connection strength if the materials used in the connection are weaker than the expected strengths.

For design applications, the specified minimum nominal strengths of the materials can be used along with the applicable reduction factors on the component strength calculations. Use of nominal material strengths and reduction factors in the model results in connection strengths that are consistent with the existing connection limit state calculations in the Steel Construction Manual (AISC 2011).

CALCULATION OF CONNECTION RESPONSE QUANTITIES

While the component-based model for single plate shear connections can be incorporated into a general finite element analysis using a variety of commercial software, here the

component-based model is implemented using a rigid-body displacement model to relate the connection demands to the connection spring displacements. In this approach, the responses of the connections are calculable via spreadsheet, and thus specialized analysis software is not required.

Calculation of Component Spring Displacements from Connection Demands

The axial deformations of the connection springs, Δ_{j}, are calculated in terms of the connection rotation and axial deformation demands, θ and δ, respectively, using a rigid-body fiber-displacement model derived by Weigand and Berman (2014):

$$\Delta_{\mathrm{j}} = \delta + (1 - \cos\theta)\, X_{\mathrm{j1}} - \sin\theta X_{\mathrm{j2}} \tag{25}$$

where $\mathbf{X}_{\mathrm{j}}$ denotes the location of the j^{th} connection spring with components $\mathbf{X}_{\mathrm{j}} = \{X_{\mathrm{j1}}, X_{\mathrm{j2}}\}^T$ relative to the center of rotation of the connection (Fig. 12). For seismic tests, the connections are subjected only to rotation demands (i.e., $\delta = 0$), and thus the connection spring deformations are essentially linear with increasing rotation (Fig. 13(a)).

For the connections subjected to column removal, the connection demands are calculated by assuming that the connections are part of two-span system where (i) the removed column remains vertical as it deflects downward, and (ii) all deformations occur at the connections (Fig. 14(a)). Using these assumptions, the rotation demand is related to the vertical deflection of the simulated missing column (termed 'simulated vertical displacement'), Δ_{syst}, as:

$$\theta = \tan^{-1}\left(\frac{\Delta_{\mathrm{syst}}}{L_{\mathrm{r}}}\right) \quad , \tag{26}$$

where L_{r} is the distance between the centers of gravity of connection bolt groups on the ends of the framing members in the undeformed configuration. The connection axial deformation

demand, δ, can also be related to the simulated vertical displacement as

$$\delta = \frac{L_{\mathrm{r}}}{2}\left[\sqrt{1+\left(\frac{\Delta_{\mathrm{syst}}}{L_{\mathrm{r}}}\right)^{2}}-1\right] \quad , \tag{27}$$

in which δ is always aligned with the centerline of the deflected framing member. Fig. 13(b) shows an example of the connection spring displacements calculated under column removal, using the connection demands in Eqs. (26) and (27).

The division of the connection spring displacement among the component springs is calculated incrementally. For each connection spring, the incremental displacement of the component springs resulting from the i^{th} displacement increment is calculated using the component spring tangent stiffnesses at the beginning of the displacement increment (denoted $K_{T,plt}^{i-1}$, $K_{T,bw}^{i-1}$, and $K_{T,bolt}^{i-1}$ for the shear plate, beam web, and bolt, respectively) such that:

$$\Delta_{\mathrm{j,plt}}^{\mathrm{i}} = \Delta_{\mathrm{j,plt}}^{\mathrm{i\text{-}1}} + \frac{K_{T,bw}^{i-1}K_{T,bolt}^{i-1}}{K_{T,plt}^{i-1}K_{T,bw}^{i-1}+K_{T,bw}^{i-1}K_{T,bolt}^{i-1}+K_{T,plt}^{i-1}K_{T,bolt}^{i-1}}\left(\Delta_{\mathrm{j}}^{\mathrm{i}}-\Delta_{\mathrm{j}}^{\mathrm{i\text{-}1}}\right) \tag{28a}$$

$$\Delta_{\mathrm{j,bw}}^{\mathrm{i}} = \Delta_{\mathrm{j,bw}}^{\mathrm{i\text{-}1}} + \frac{K_{T,plt}^{i-1}K_{T,bolt}^{i-1}}{K_{T,plt}^{i-1}K_{T,bw}^{i-1}+K_{T,bw}^{i-1}K_{T,bolt}^{i-1}+K_{T,plt}^{i-1}K_{T,bolt}^{i-1}}\left(\Delta_{\mathrm{j}}^{\mathrm{i}}-\Delta_{\mathrm{j}}^{\mathrm{i\text{-}1}}\right) \tag{28b}$$

$$\Delta_{\mathrm{j,bolt}}^{\mathrm{i}} = \Delta_{\mathrm{j,bolt}}^{\mathrm{i\text{-}1}} + \frac{K_{T,plt}^{i-1}K_{T,bw}^{i-1}}{K_{T,plt}^{i-1}K_{T,bw}^{i-1}+K_{T,bw}^{i-1}K_{T,bolt}^{i-1}+K_{T,plt}^{i-1}K_{T,bolt}^{i-1}}\left(\Delta_{\mathrm{j}}^{\mathrm{i}}-\Delta_{\mathrm{j}}^{\mathrm{i\text{-}1}}\right) \tag{28c}$$

where $\Delta_{\mathrm{j,plt}}^{\mathrm{i}}$, $\Delta_{\mathrm{j,bw}}^{\mathrm{i}}$, and $\Delta_{\mathrm{j,bolt}}^{\mathrm{i}}$ are the current displacements of the shear plate, beam web, and bolt, respectively, $\Delta_{\mathrm{j,plt}}^{\mathrm{i\text{-}1}}$, $\Delta_{\mathrm{j,bw}}^{\mathrm{i\text{-}1}}$, and $\Delta_{\mathrm{j,bolt}}^{\mathrm{i\text{-}1}}$ are the previous displacements of the shear plate, beam web, and bolt, respectively. With component spring deformations calculated via Eq. (28), the model displacement response can be calculated explicitly in terms of the connection and system geometry and the imposed rotation or vertical column deflection.

Calculation of Connection Resistance

The vertical resistance of the component-based connection model is calculated as if the connection were part of the two-span system described above, subjected to a concentrated load at the interior column in the two-span system (Fig. 14(b)). The concentrated load at

the interior column is related to the connection forces by summing forces in the vertical direction such that

$$\begin{aligned} P &= 2\left(V_{\mathrm{c}}\cos\theta + T_{\mathrm{c}}\sin\theta\right) \\ &= 2\left(\frac{2M_{\mathrm{c}}}{L_{\mathrm{r}}}\cos\theta + T_{\mathrm{c}}\sin\theta\right) \quad , \end{aligned} \tag{29}$$

where $V_{\mathrm{c}} = \frac{2M_{\mathrm{c}}}{L_{\mathrm{r}}+2\delta} \approx \frac{2M_{\mathrm{c}}}{L_{\mathrm{r}}}$ is the connection shear force, $T_{\mathrm{c}} = \sum_{\mathrm{i}}^{n_{\mathrm{cs}}} R_{\mathrm{i}}(d_{\mathrm{i,axial}})$ is the connection tensile force, and $M_{\mathrm{c}} = \sum_{\mathrm{i}}^{n_{\mathrm{cs}}} R_{\mathrm{i}}(d_{\mathrm{i,axial}})X_{\mathrm{i2}}$ is the connection moment.

MODEL RESULTS AND VALIDATION

Validation against Connection Test under Seismic Loads

The moment-rotation response shown in Fig. 10 was calibrated to the data from Liu and Astaneh-Asl (2004), in order to determine the pinching behavior at large rotations. That comparison is not sufficient to validate the component-based model, and thus the model was also compared to data from Crocker and Chambers (2000), for a 4-bolt single-plate shear connection with 19.1 mm (3⁄4 in) diameter A325 bolts, a 9.53 mm (3⁄8 in) thick A36 shear plate, and a W18×55 beam section. Crocker and Chambers (2000) list the material grades, but does not include coupon data for the shear plate and beam web materials. For the component-based model, the plate material yield and ultimate tensile strengths were taken as equal to the expected material strengths from ANSI/AISC 341-10 (AISC 2005).

The component-based model was subjected to pure rotation cycles, with the same peak rotations values as were used in the test. Fig. 15 shows a comparison of the predicted response calculated via the model to the moments at the peak rotations from each cycle. The model underestimated the initial resistance of the connection at small rotations, relative to the connection data, but started to better approximate the peak moments of the connection at large rotations. During the last cycle prior to connection failure in the test, the model response matched the moments at the peak connection rotations within 5 % (4 % at the cycle peak and 1 % at the cycle valley). Fig. 15 demonstrates that the component-based model

can reasonably predict peak moment-rotation behavior for a single-plate shear connection under seismic loads.

Validation against Connection Tests under Column Removal

To examine the ability of the model to capture the connection behavior under column removal, the component-based connection model was compared to 13 single-plate shear connection sub-assemblages tested by Weigand and Berman (2014) under simulated column removal. The naming convention for the specimens follows the convention outlined in Weigand and Berman (2014), which consists of a prefix that describes the connection type (e.g, sps (Single-Plate Shear)), followed by the number of bolts (e.g., 3b corresponds to three bolts), the hole type (e.g., STD), bolt diameter fraction in inches (e.g., 34 corresponds to 3/4 in. (19.1 mm)), plate thickness fraction (e.g., 38 corresponds to ⅜ in (9.53 mm)), and additional descriptor (e.g., Edge) where applicable. Each of the connection sub-assemblages consisted of a 1524 mm (60.0 in) long column stub and a 1220 mm (48.0 in) long beam stub connection via a single-plate shear connection whose geometry was varied between tests. The connection parameters varied between tests included the number of bolts, bolt diameter, bolt grade, plate thickness, horizontal plate edge distance, hole type (Standard or Short-Slotted), eccentricity with respect to the beam centerline, and the simulated system span. More information on the geometries of the connection sub-assemblages is available in Weigand and Berman (2014).

To model the responses of the 13 connections tested under column removal to complete failure, the limit states of bolt shear and plate tearout (of the shear plate and beam web edge distances) were incorporated into the connection models. Bolt shear was enforced as a deformation limit with a constant limiting bolt deformation value of 3.18 mm (0.125 in) for A325 bolts and a constant value of 2.67 mm (0.105 in) for A490 bolts, based on measured bearing deformations in the bolts from single-plate shear connections subjected to simulated column removal loading (reported in Weigand (2014)). Plate tearout was also enforced as a deformation limit, because it controlled in 3 of the 13 tests. However, due to the limited

data on plate deformations at the connection bolt widths prior to failure, the values for the limiting plate deformations were calibrated against the individual connection tests controlled by tearout. Therefore the response of Specimens sps3b|SSLT|34|38|Edge, sps3b|SSLT|34|14|, and sps3b|SSLT|34|14|Weak, which were each controlled by tearout, should only be considered as validated prior to the peak load. From the calibrated data, the plate clear distance appears to provide a reasonable estimate of the plate deformation capacity in tension, however more data would be needed to fully characterize the plate tearout deformation capacity for the range of bolt diameters and plate thicknesses used for single-plate shear connections in practice.

The model is subjected to the same rotation and axial deformation demands as were used in the sub-assemblage tests; however, for the tested connections, those demands were applied via a load beam at a distance from the connection that was significantly smaller than the simulated span, in effect inducing excess shear on the connection (the reaction frame and loading protocol used in the connection tests was designed to apply the appropriate rotation and axial deformation demands on the connection sub-assemblages, as if they were part of the larger two-span system shown in Fig. 14). The component spring displacements, due to the connection demands, were calculated from Eq. (28). Fig. 16 shows a comparison of the model prediction with the vertical and horizontal force-displacement responses from Specimen sps4b|STD|34|38|48L from Weigand and Berman (2014), which corresponds to a 4-bolt single-plate shear connection with 19.1 mm (3⁄4 in) bolts, a 9.53 mm (3⁄8 in) thick shear plate, and a 14.6 m (48 ft) simulated span. These plots show that the component-based model was able to reasonably predict the general characteristics and capacity of the vertical force-displacement response and to very closely predict the horizontal force-displacement response.

The model under-predicts the connection vertical load throughout most of the analysis, relative to the connection data. This discrepancy occurs as a result of the excess shear force in the tested connections, as described above. The model does not account for this

excess shear force; however, as the excess shear force dissipates at large simulated vertical displacements, when the shear load on the connection is primarily a result of tension in the rotated configuration, the vertical force-displacement response of the model can be expected to approach that of the tested connection. Fig. 16(a) thus shows that the model exhibits the expected behavior, approaching the vertical force-displacement response of the tested connections at large rotations.

Fig. 16 also demonstrates that the model was able to qualitatively capture the connection degradation response until complete connection failure. The model systematically predicts more gradual progressions of bolt shear occurrences than were observed in the tests. This results from the use of the rigid-body deformation model to calculate the connection spring displacements. The rigid-body model was intended to be simple and does not account for the redistribution of flexural loads that occurs after the sequential component failures. Thus the rigid-body model cannot capture the resulting increases in the rates of accumulation of axial deformations among the remaining bolts with simulated vertical displacement when failure occurs. However, the component-based connection model is equally capable of being incorporated into a more general nonlinear finite element program, and that model should be able to more accurately capture the connection degradation, as it would correctly account for the redistribution of loads when connection failure occurs.

Fig. 17 shows a complete set of comparisons between the model and the vertical and horizontal force-displacement responses of the connections tested by Weigand and Berman (2014), and Table 1 compiles the axial fiber displacements computed from the model and from the experiments at the instance of connection failure (i.e., maximum vertical resistance), as well as the percent difference between the two displacement measures. These comparisons show that the model was able to capture the overall behavior of the connections, and to predict the peak vertical and horizontal connection capacities within an average of 8.5 % and 4.4 %, respectively. This agreement between the model and the experiments serves as validation that the presented modeling approach can adequately predict the behavior of

single-plate shear connections subjected to column removal, in terms of both their qualitative behavior and their peak load and deformation capacities.

ASSUMPTIONS AND LIMITATIONS

The proposed component-based modeling approach provides accurate coupling between the in-plane flexural and axial behaviors of a connection, based on an approximation in which a discrete spring is used to represent the axial load-deformation behavior of each bolt row, as described in the *Component-based Connection Model* Section. The influence of vertical shear force on the axial behavior of the connection springs is neglected, as the model is intended for cases in which shear demands are small relative to the flexural and axial demands. These approximations are consistent with component-based formulations presented by others (e.g., Wales and Rossow (1983), Richard et al. (1988)) and are appropriate for each of the validation cases considered in this study, as the connections were subjected to predominantly in-plane flexural and axial loads.

Limiting deformations measured from tests of single-plate shear connections by Weigand and Berman (2014) were used as failure criteria in the component-based modeling. The deformation limits of individual connection components depend on both the material properties and the geometry of the connections that were tested, so caution should be exercised in applying these deformation limits for other materials and connection geometries. Global connection-level limit states, such as net-section tensile rupture of the shear plate or block-shear rupture of the beam web, were not incorporated; however, such limit states are not likely to control for conventional steel gravity connections under flexural and axial loads. Binding contact between the beam flange and the column flange was not considered in this study, but this effect can be readily incorporated using stiff compression-only springs at the beam flanges (e.g., Main and Sadek (2012)).

SUMMARY AND CONCLUSIONS

This paper has described the development of a new component-based model for single-plate shear connections. By aggregating the force-displacement behaviors of the individual

connection components (i.e., the bolt, shear plate, and beam web), the model was shown to capture relatively complex connection behaviors and failure modes, including bolt shear and plate tearout. The model was compared against the moment-rotation response of single-plate shear connections tested under increasing magnitude rotation cycles (i.e., seismic loads), as well as against the vertical and horizontal force-displacement responses of connections tested under combined rotation and axial deformation demands (i.e., column removal loads). The close agreement between the model and the connection experiments serves as validation of the proposed modeling approach. The component-based model was able to predict the capacities of 13 single-plate shear connection configurations within an average of 10 %, using the connection geometry, material properties, and applied loading.

Beyond the connection tests considered in this paper for the validation, the component-based model described herein provides new capabilities, such as accurate modeling of the peak connection performance and energy dissipation capacity, that are critical to accurately modeling the response of connections subjected to extreme loads. The effects of pre-tension in the bolts are incorporated directly into the model, allowing the force-displacement behavior of connections with slip-critical bolts and snug-tight bolts to be differentiated. The model also allows direct modeling of the effects of both standard (STD) and slotted (SSLT, LSLT) holes, and captures their associated influence on the connection capacity under column removal. Finally, the model accounts for load reversals and the pinching effects associated with hysteresis, which are critical to modeling the history-dependent resistance and energy dissipation capacity of connections under seismic loads, and which also play a role in the behavior of single-plate shear connections subjected to column removal.

ACKNOWLEDGMENTS

Jonathan M. Weigand performed this work during his tenure as a NIST/NRC Postdoctoral Research Associate. The author would like to sincerely thank and acknowledge his NRC Postdoctoral Research Adviser, Dr. Joseph A. Main of the National Institute of Standards and Technology, for his guidance and valuable feedback on this work.

DISCLAIMER

Certain commercial entities, equipment, products, or materials are identified in this document in order to describe a procedure or concept adequately. Such identification is not intended to imply recommendation, endorsement, or implication that the entities, products, materials, or equipment are necessarily the best available for the purpose.

REFERENCES

AISC (2005). *Seismic Provisions for Structural Steel Buildings*. American Institute of Steel Construction, Inc.

AISC (2011). *Steel Construction Manual*. American Institute of Steel Construction, Chicago, IL, 14 edition.

Astaneh-Asl, A. (2005). *Design of Shear Tab Connections for Gravity and Seismic Loads*. University of California at Berkeley, Berkeley, CA.

ASTM (2014a). *Standard Specification for High-Strength Steel Bolts, Classes 10.9 and 10.3, for Structural Steel Joints (Metric)*. American Society for Testing and Materials (ASTM) International, West Conshohocken, PA.

ASTM (2014b). *Standard Specification for Structural Bolts, Heat Treated 830 MPa Minimum Tensile Strength (Metric)*. American Society for Testing and Materials (ASTM) International, West Conshohocken, PA.

Crocker, J. and Chambers, J. (2000). "Single plate shear connection response to rotation demands imposed by frames undergoing cyclic lateral displacements." *Journal of Structural Engineering*, 130(6), 934–941.

Crocker, J. and Chambers, J. (2004). "Single plate shear connection response to rotation demands imposed by frames undergoing cyclic lateral displacements." *Journal of Structural Engineering*, 130(6), 934–941.

Elsati, M. K. and Richard, R. M. (1996). "Derived moment rotation curves for partially restrained connections." *Structural Engineering Review*, 8(2/3), 151–158.

Farin, G. (1993). *Curves and surfaces for computer aided geometric design. A practical guide.* Academic Press.

Foley, C. M., Martin, K., and Schneeman, C. (2006). "Robustness in structural steel framing systems." *Report No. MU-CEEN-SE-06-01*, Marquette University.

Giuffré, A. and Pinto, P. E. (1970). "Il comportamento del cemento armato per sollecitazioni cicliche di forte intensitá." *Giornale del Genio Civile*, 101, 391–408.

Grondin, G., Jin, M., and Josi, G. (2007). "Slip critical bolted connections-a reliability analysis for design at the ultimate limit state." *Report No. Structural Engineering Report 274*, University of Alberta.

Hsieh, S. H. and Deierlein, G. G. (1990). "Nonlinear analysis of three-dimensional steel frames with semi-rigid connections." *Computers & Structures*, 41(5), 995–1009.

Johnson, E. S. and Meissner, J. E. Fahnestock, L. A. (2015). "Experimental behavior of a large-scale steel-concrete composite floor system subjected to column removal scenarios." *Journal of Structural Engineering.*

Johnson, E. S., Weigand, J. M., Francisco, T., Fahnestock, L. A., Liu, J., and Berman, J. W. (2014). "Large-Scale Experimental Evaluation of the Structural Integrity of a Composite Steel and Concrete Building Floor System." *ASCE/SEI Structures Congress*, Boston, MA (April).

Judd, J. P. and Charney, F. A. (2014). "Seismic collapse prevention systems." *Tenth U.S. National Conference on Earthquake Engineering*, Anchorage, AK (July 21–25).

Koduru, S. D. and Driver, R. G. (2014). "Generalized component-based model for shear tab connections." *Journal of Structural Engineering*, 04013041–1–10.

Liu, J. and Astaneh-Asl, A. (1999). "Cyclic Testing of Simple Connections Including Slab Effects, Volume I: Results of Test Series "A"." *Report No. UCB/CEE-Steel-99/01*, University of California at Berkeley.

Liu, J. and Astaneh-Asl, A. (2004). "Moment-rotation parameters for composite shear tab connections." *Journal of Structural Engineering*, 130(9), 1371–1380.

Main, J. A. and Sadek, F. (2012). "Robustness of steel gravity frame systems with single-plate shear connections." *Report No. NIST-TN-1749*, National Institute of Standards and Technology, United States Department of Commerce.

Main, J. A. and Sadek, F. (2014). "Modeling and analysis of single-plate shear connections under column loss." *Journal of Structural Engineering*, 140(3), 04013070.

Menegotto, M. and Pinto, P. E. (1973). "Method of analysis of cyclically loaded reinforced concrete plane frames including changes in geometry and nonelastic behavior of elements under combined normal geometry and nonelastic behavior of elements under combined normal force and bending." *Proceedings of the IABSE Symposium on the Resistance and Ultimate Deformability of Structures Acted on by Well-Defined Repeated Loads*, Lisbon, PT.

Nelson, W. D., Bunin, B. L., and Hart-Smith, L. J. (1983). "Critical joints in large composite aircraft structure." *Report No. NASA Contractor Report 3710*, Douglas Aircraft Company, McDonnell Douglas Corporation.

Oosterhof, S. A. and Driver, R. G. (2012). "Performance of Steel Shear Connections under Combined Moment, Shear, and Tension." *ASCE/SEI Structures Congress*, Chicago, IL, 146–157 (March).

Prautizsch, H., Boehm, W., and Paluszny, M. (2002). *Bézier and B-Spline Techniques*. Springer Science & Business Media.

Ramberg, W. and Osgood, W. T. (1943). "Description of stress-strain curves by three parameters." *Report no.*, NACA, Washington, D.C.

Rassati, G. A., Leon, R. T., and Noe, S. (2004). "Component Modeling of Partially Restrained Composite Joints Under Cyclic and Dynamic Loading." *Journal of Structural Engineering*, 130(2), 343–351.

Rex, C. O. and Easterling, W. S. (1996). "Behavior and modeling of a single plate bearing

730 on a single bolt." *Report No. CE/VPI-ST 96/14*, Virginia Polytechnic Institute and State
731 University.
732 Richard, R. M. and Abbott, B. J. (1975). "Versatile elastic-plastic stress-strain formulation."
733 *Journal of the Engineering Mechanics*, 101(EM4), 511–515.
734 Richard, R. M., Wei-Kung, H., and M., C. (1988). "Derived moment rotation curves for
735 double framing angles." *Computers & Structures*, 30(3), 485–494.
736 Sadek, F., El-Tawil, S., and Lew, H. S. (2008). "Robustness of composite floor systems with
737 shear connections: Modeling, simulation, and evaluation." *Journal of Structural Engineer-*
738 *ing*, 134(11), 1717–1725.
739 Shen, J. and Astaneh-Asl, A. (2000). "Hysteresis model of bolted-angle connections." *Journal*
740 *of Constructional Steel Research*, 54, 317–343.
741 Simões, R., Simões da Silva, L., and Cruz, P. (2001). "Cyclic behaviour of end-plate beam-
742 to-column composite joints." *Steel and Composite Structures*, 1(3), 355–376.
743 Thomas, D. L., Wilson, J. M., and Wilson, R. R. (1973). "Timoshenko beam finite elements."
744 *Journal of Sound and Vibration*, 31(3), 315–330.
745 Thompson, S. L. (2009). "Axial, shear and moment interaction of single plate "shear tab"
746 connections." Ph.D. thesis, Milwaukee School of Engineering, Milwaukee School of Engi-
747 neering (May).
748 Wales, M. W. and Rossow, E. C. (1983). "Coupled moment-axial force behavior in bolted
749 joints." *Journal of Structural Engineering*, 109(5), 1250–1266.
750 Weigand, J. M. (2014). "The Integrity of Steel Gravity Framing System Connections Sub-
751 jected to Column Removal Loading." Ph.D. Dissertation in Civil Engineering, University
752 of Washington, Seattle, WA (June).
753 Weigand, J. M. and Berman, J. W. (2008). "Rotation and strength demands for simple
754 connections to support large vertical deflections." *World Conference on Earthquake Engi-*
755 *neering*, Beijing, China.
756 Weigand, J. M. and Berman, J. W. (2014). "Integrity of Steel Single Plate Shear Connections

Subjected to Simulated Column Removal." *Journal of Structural Engineering*, 140(5).

Wen, R., Akbas, B., and Shen, J. (2013a). "Practical moment-rotation relations of steel shear tab connections." *Journal of Constructional Steel Research*, 88, 296–308.

Wen, R., Akbas, B., Sutchiewcharn, N., and Shen, J. (2013b). "Inelastic behaviors of steel shear tab connections." *The Structural Design of Tall and Special Buildings*, 23, 929–946.

Yu, H., Burgess, I. W., Davison, J. B., and Plank, R. J. (2009). "Experimental investigation of the behaviour of fin plate connections in fire." *Journal of Constructional Steel Research*, 723–736.

List of Tables

TABLE 1: Comparison of peak vertical and horizontal connection resistances calculated from model with experimental data.

Specimen Name	V_{test} kN (kip)	V_{model} kN (kip)	% Diff. -	T_{test} kN (kip)	T_{model} kN (kip)	% Diff. -
sps3b|STD|34|38|48L	41.2 (9.26)	41.3 (9.27)	0.2	497 (111.8)	499 (112.2)	0.3
sps4b|STD|34|38|48L	55.1 (12.38)	57.0 (12.81)	3.4	647 (145.5)	651 (146.3)	0.5
sps3b|STD|34|38|	40.2 (9.05)	45.1 (10.14)	12.1	496 (111.5)	479 (107.6)	3.5
sps3b|SSLT|34|38|	44.1 (9.90)	48.9 (11.00)	11.1	474 (106.5)	465 (104.5)	1.9
sps3b|SSLT|34|38|Edge	32.3 (7.26)	32.7 (7.36)	1.3	384 (86.3)	339 (76.2)	11.7
sps4b|SSLT|34|38|	49.6 (11.15)	56.0 (12.58)	12.9	544 (122.3)	514 (115.6)	5.5
sps5b|SSLT|34|38|	60.4 (13.57)	63.4 (14.25)	5.0	631 (141.8)	619 (139.2)	1.8
sps3b|SSLT|34|38|A490	52.4 (11.78)	57.0 (12.81)	8.8	527 (118.4)	524 (117.8)	0.5
sps3b|SSLT|34|38|Offset	43.4 (9.75)	48.4 (10.87)	11.5	436 (98.0)	459 (103.1)	5.2
sps4b|SSLT|78|38|	48.7 (10.95)	53.6 (12.05)	10.1	503 (113.1)	554 (124.6)	10.2
sps3b|SSLT|34|14|	38.9 (8.75)	39.0 (8.77)	0.3	388 (87.1)	370 (83.1)	4.6
sps3b|SSLT|34|38|Gap[1]	36.9 (8.30)	-	-	427 (96.1)	-	-
sps3b|SSLT|34|14|Weak	38.5 (8.66)	41.4 (9.31)	7.5	388 (87.2)	372 (83.7)	4.1
Average			**7.0**			**4.2**

[1] Not applicable, rigid-body displacement model does not account for binding of beam flange on column flange, so it can only match this test result in an approximate sense.

List of Figures

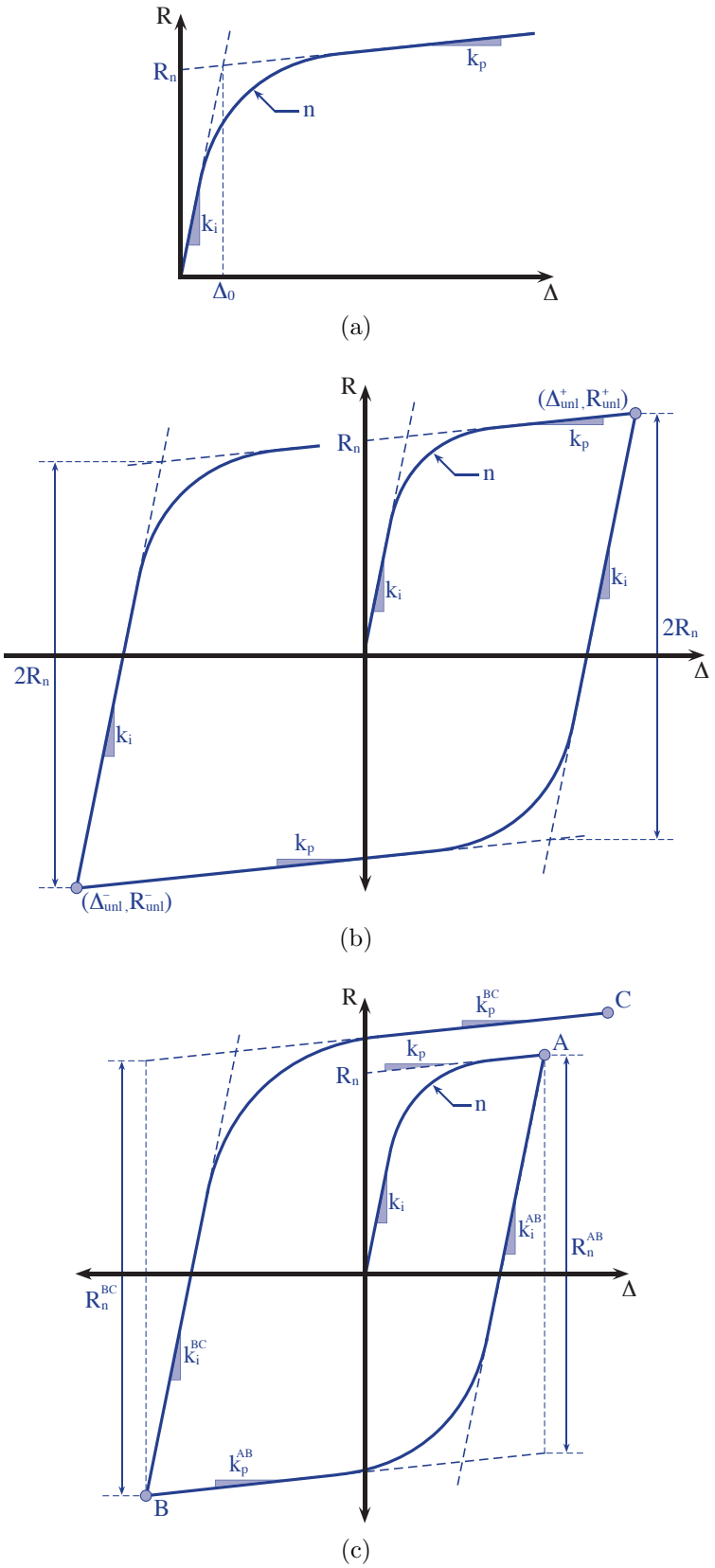

FIG. 1: Schematics for Richard Equation formulations used in (a) Richard and Abbott (1975), (b) Hsieh and Deierlein (1990), and (c) Simões et al. (2001).

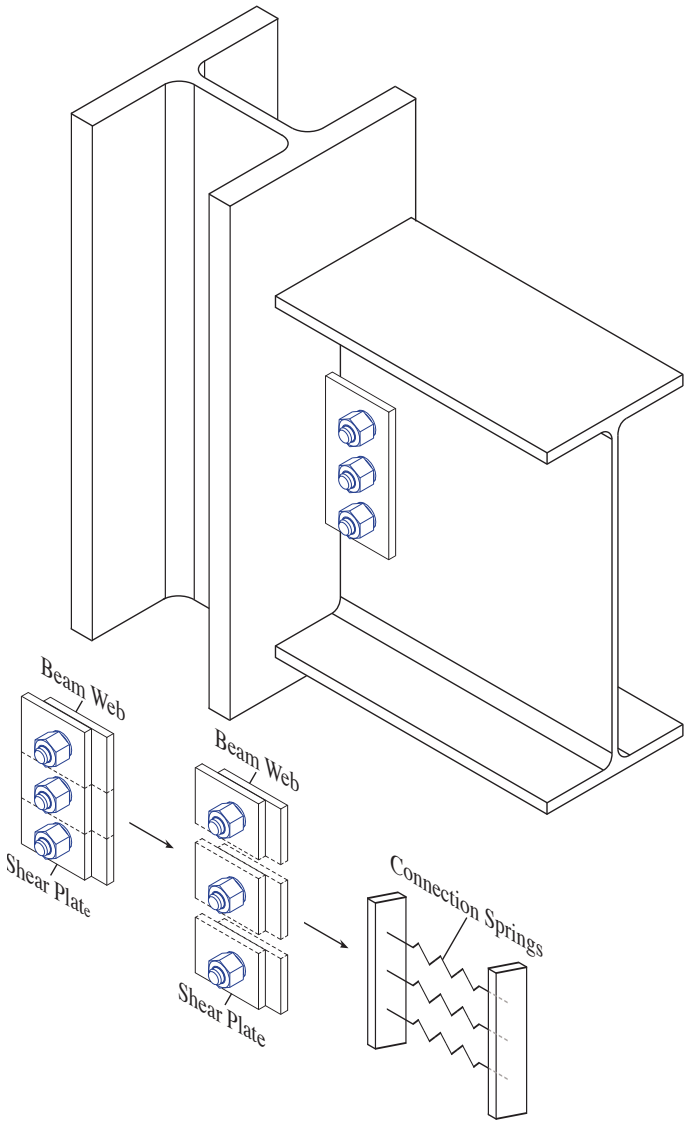

FIG. 2: Discretization of single-plate shear connection into connection springs.

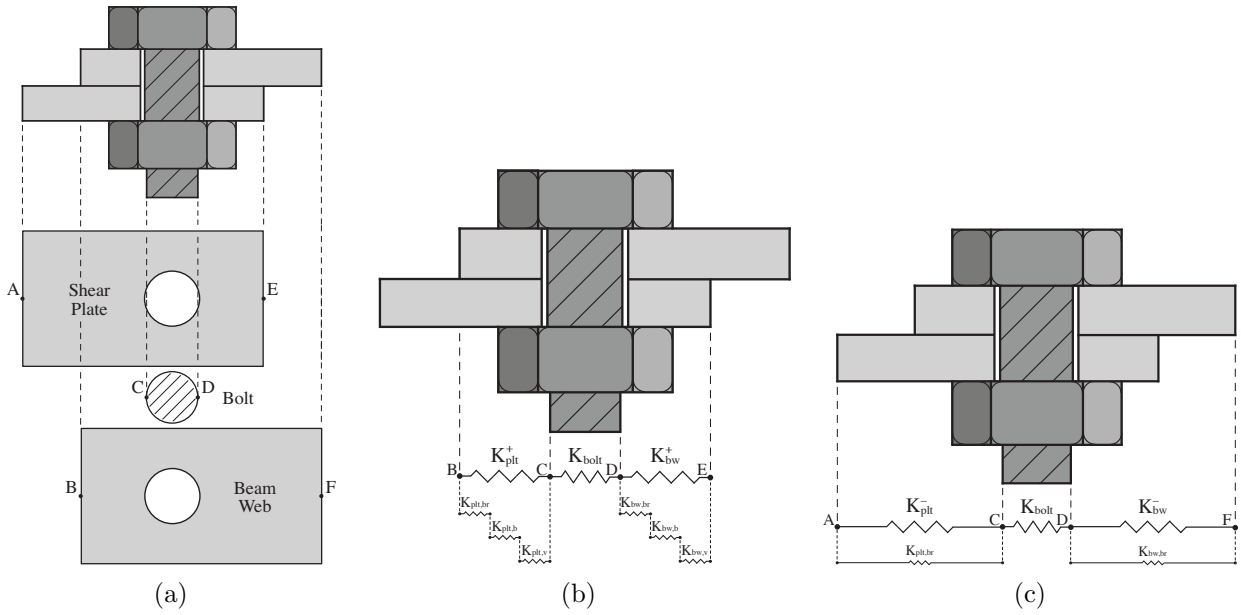

FIG. 3: Single-plate shear connection spring (a) decomposition into components, (b) stiffness contributions in tension, and (c) stiffness contributions in compression.

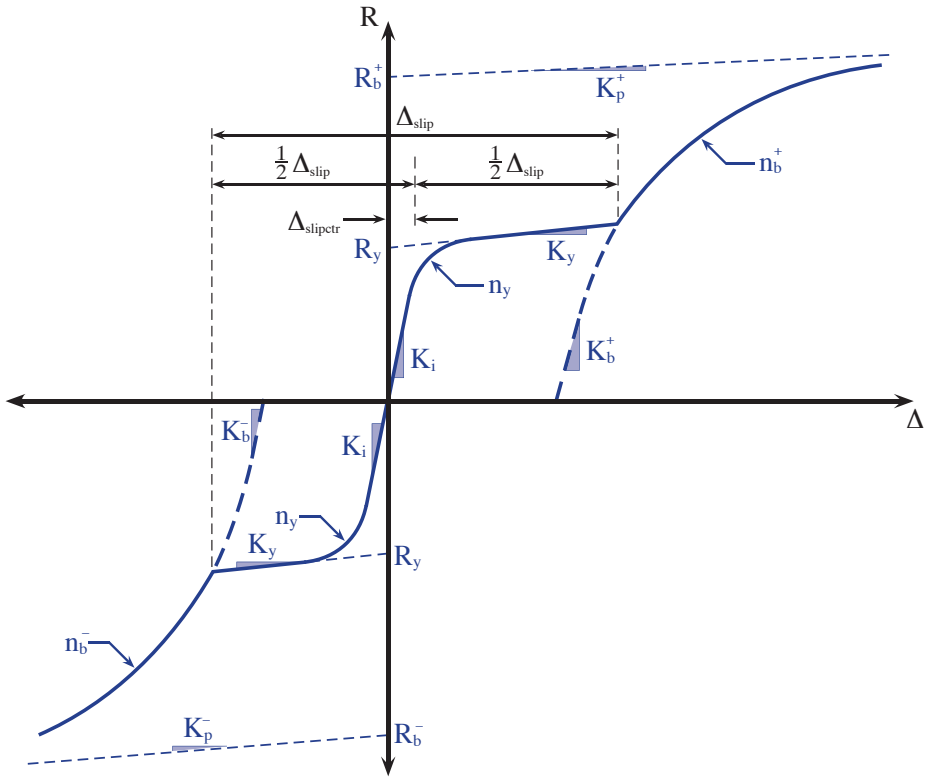

FIG. 4: Shear-plate and beam-web component spring backbone force-displacement behavior.

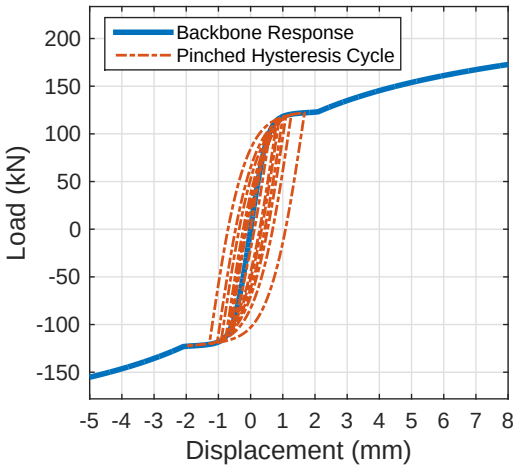

FIG. 5: Connection spring cyclic behavior prior to bearing deformations.

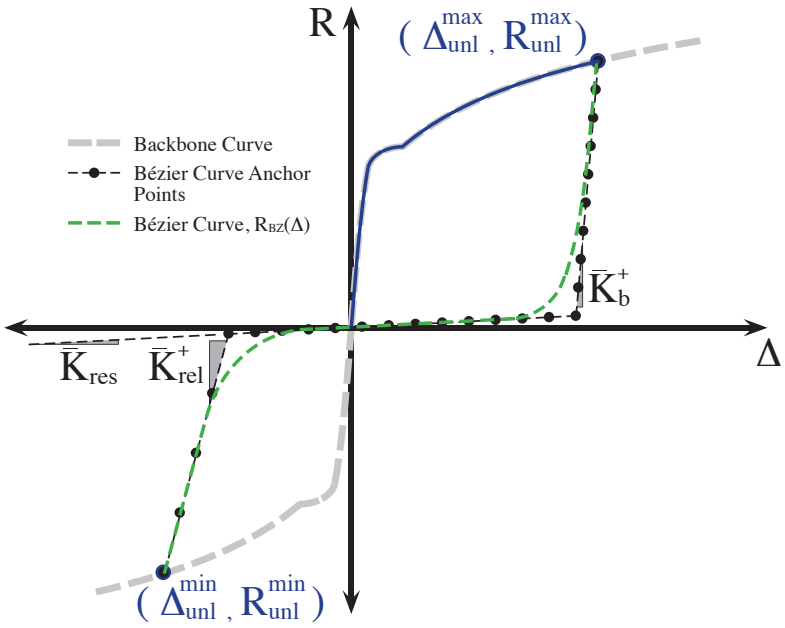

FIG. 6: Schematic of Bézier curve with control points (unload from positive deformation).

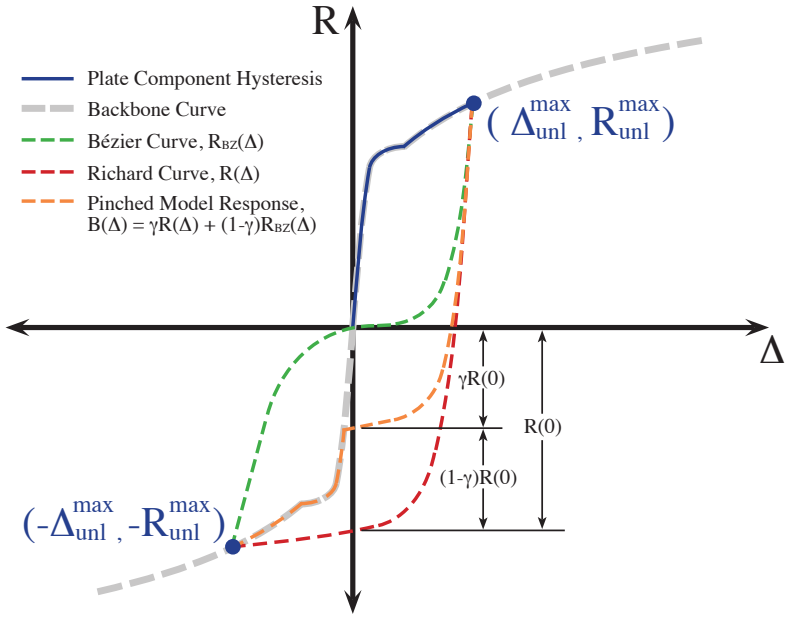

(a)

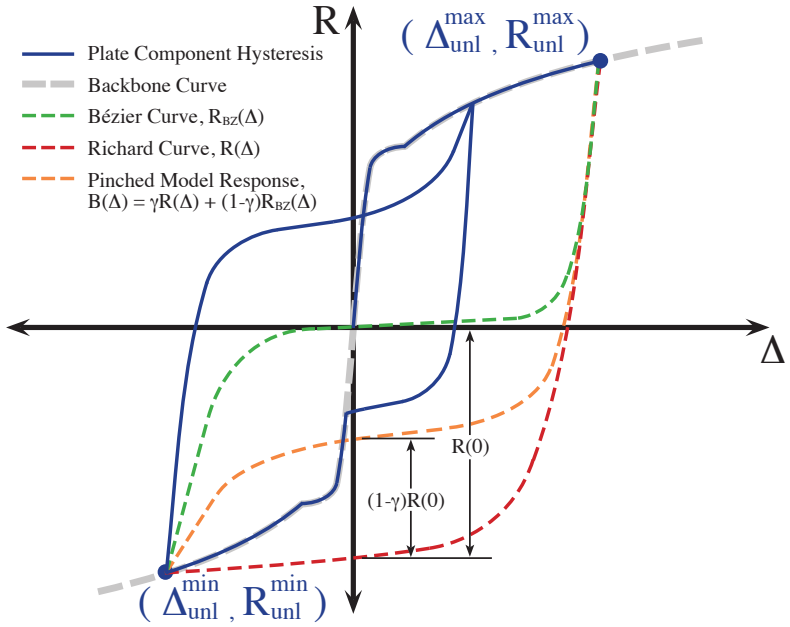

(b)

FIG. 7: Schematic showing plate component spring pinched hysteresis (Eq. (18)) for (a) initial unload cycle and (b) subsequent unload cycle.

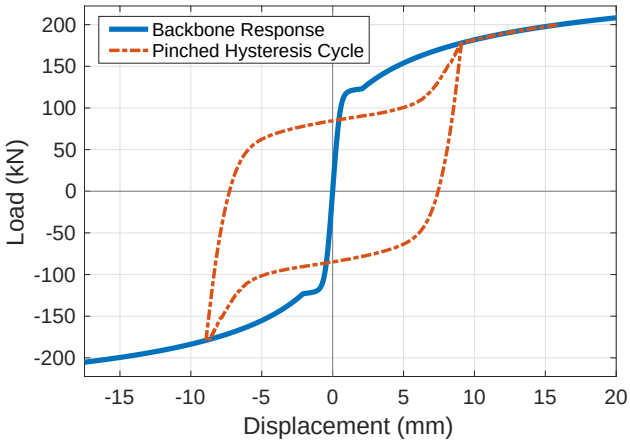

FIG. 8: Single pinched cycle pinched cycle with $\gamma = 0.5$, representative of cycle after accumulation of significant bearing deformations.

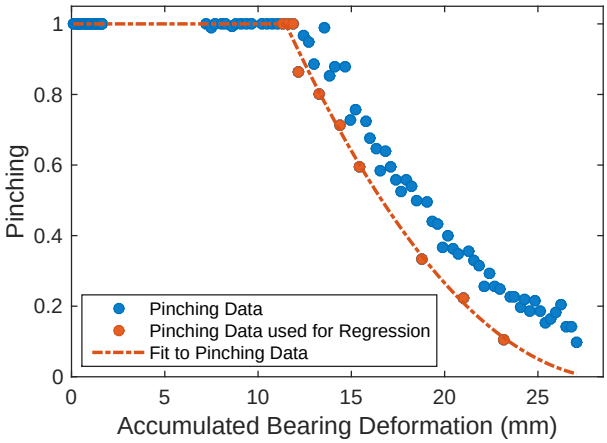

FIG. 9: Pinching ratio data with fitted pinching curve.

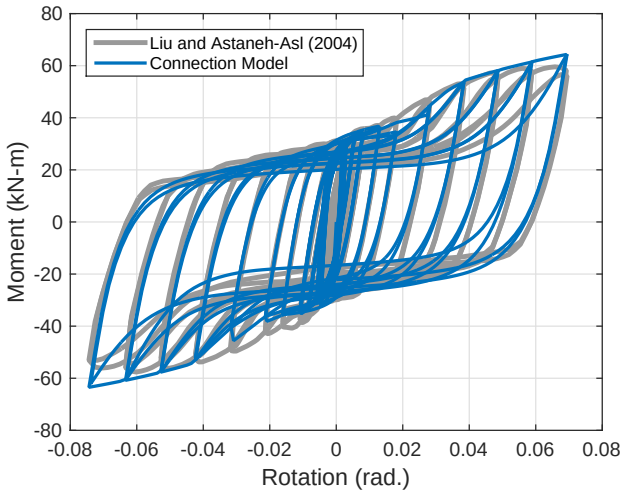

FIG. 10: Comparison of model response to experimental data from Liu and Astaneh-Asl (2004) using fitted lower-bound pinching curve.

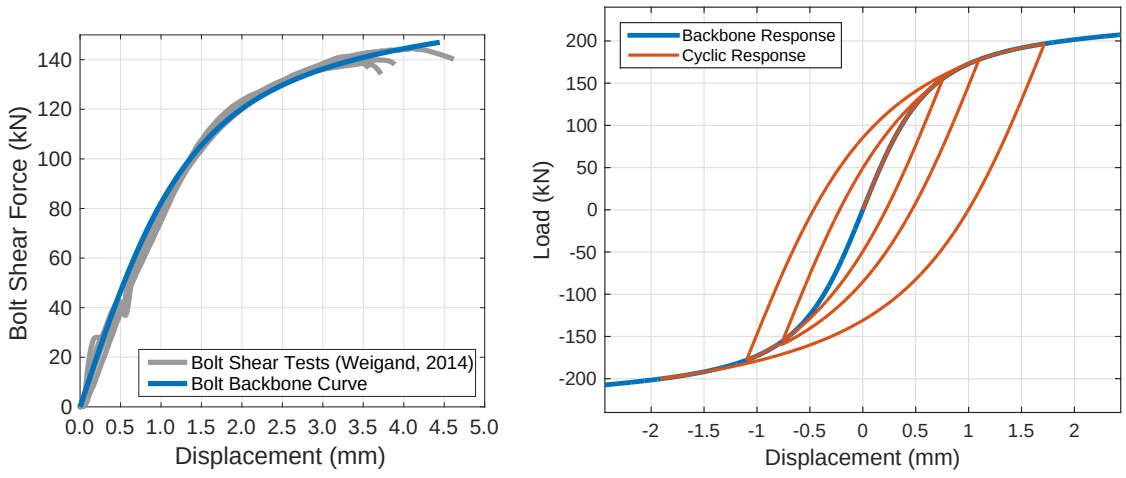

(a) (b)

FIG. 11: (a) Comparison of bolt component spring backbone response with bolt shear data from Weigand (2014), and (b) Bolt component spring cycles prior to bearing deformations.

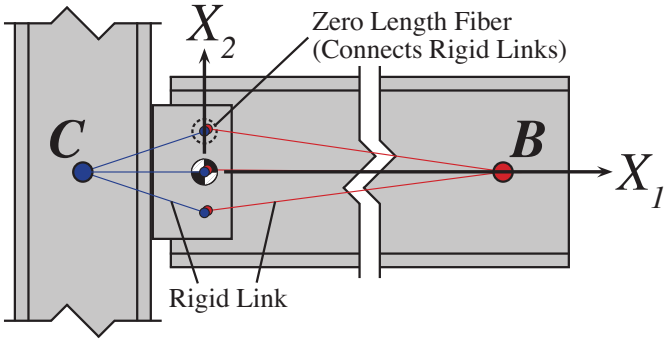

FIG. 12: Coordinate system for calculation of spring displacements from rigid-body fiber-displacement model.

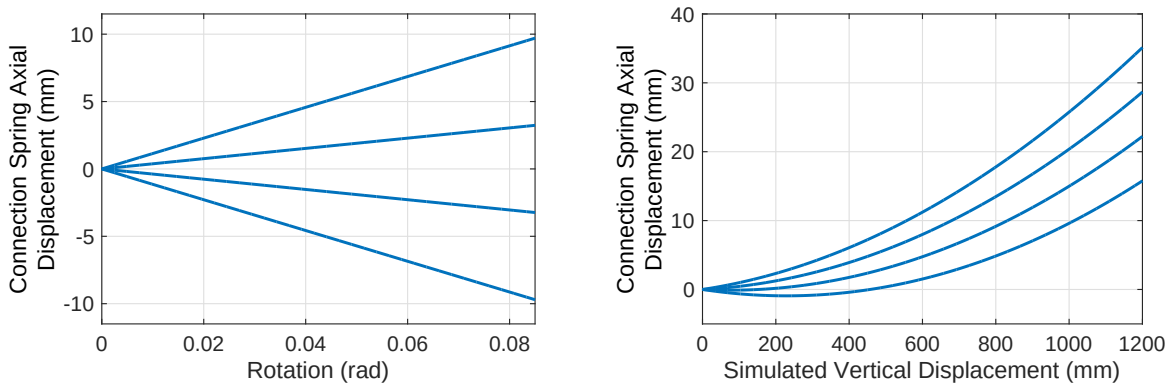

FIG. 13: Connection spring displacement profiles calculated via Eq. (25) for connection subjected to (a) rotation only and (b) rotation and axial deformation.

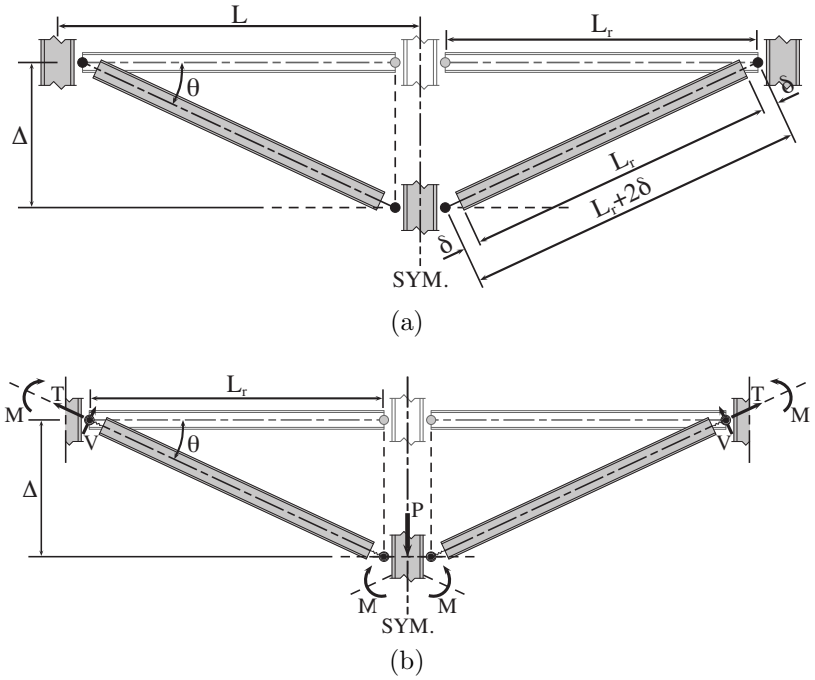

FIG. 14: Two-span system (a) deformations and (b) forces.

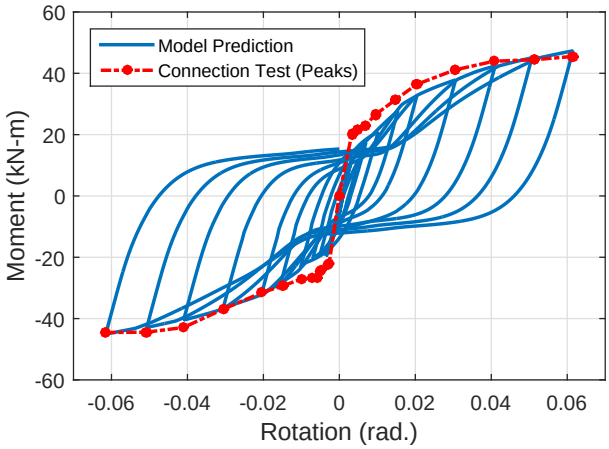

FIG. 15: Comparison of moment-rotation response predicted by component-based model with connection data (connection data shown at cycle peaks).

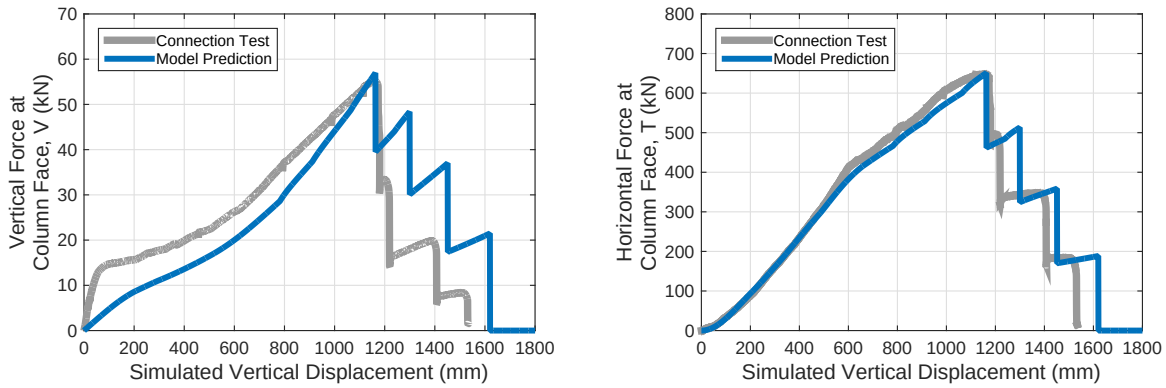

(a) (b)

FIG. 16: Comparison of predicted (a) vertical force-displacement response and (b) horizontal force-displacement response from component-based model with connection data.

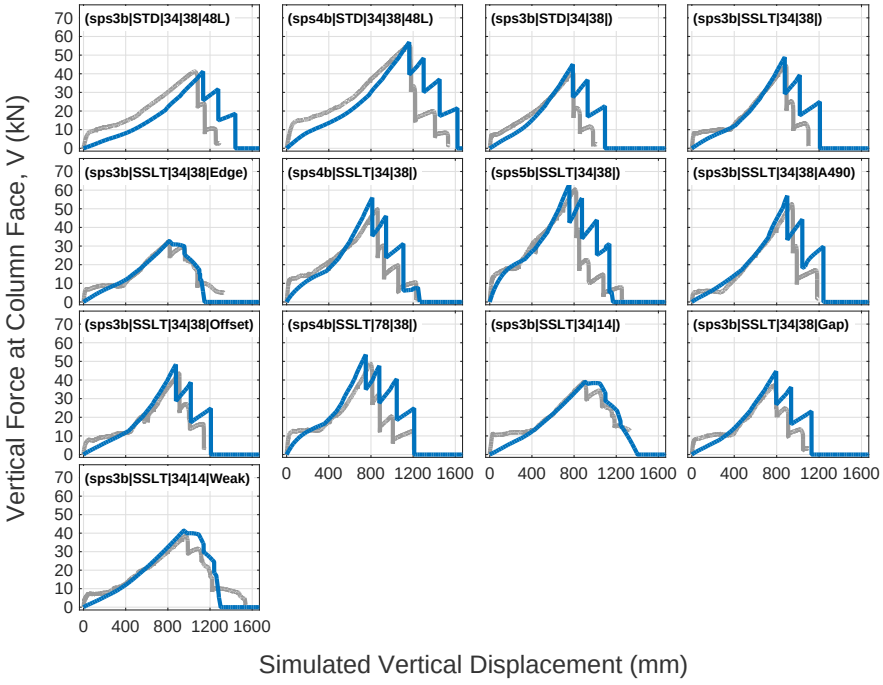

(a)

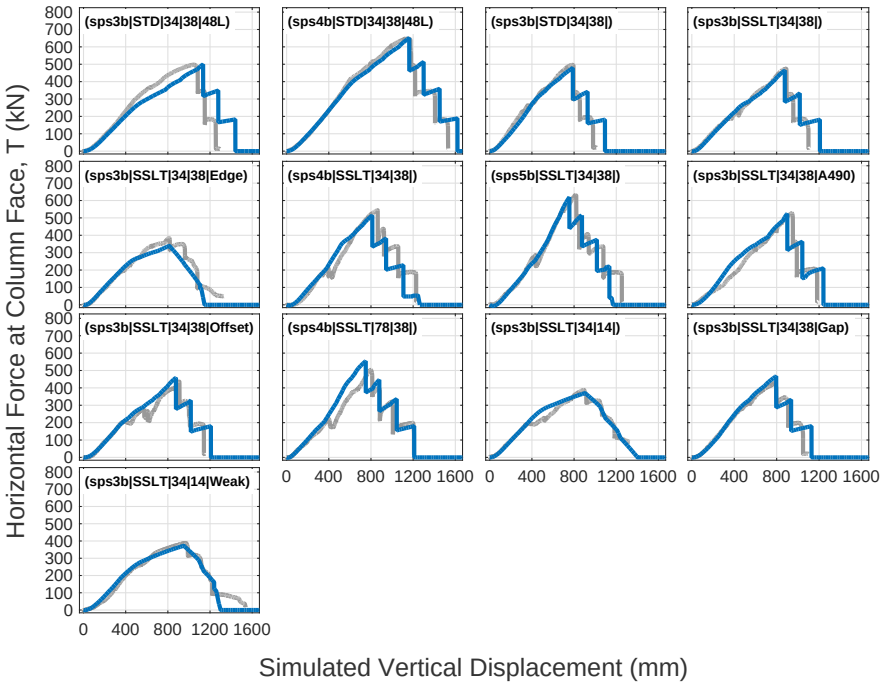

(b)

FIG. 17: Comparison of predicted response from component-based model compared to connection data.